Measurements of the Effect of Rain-Induced Sea Surface Roughness on the QuikSCAT Scatterometer Radar Cross Section

David E. Weissman, *Life Fellow, IEEE*, and Mark A. Bourassa

***Abstract*—Radar measurements of the sea surface, with satellite scatterometers that operate at K_u-band, are affected by the presence of rain through modification of the sea surface roughness by rain impacts. This is in addition to wind driven roughness, atmospheric scattering, and attenuation that affect the measured normalized radar cross section (NRCS). This paper presents a case study of the increase of the total radar cross section, averaged across surface illuminated areas (individual footprints) of the SeaWinds scatterometer (on QuikSCAT) caused by rain striking the sea surface. This effort combines satellite-based K_u-band data with high-resolution 3-D volumetric rain measurements, from simultaneous collocated Next Generation Weather Radar data. The results to be presented were acquired during a significant rain event in the Gulf of Mexico, to the east of Corpus Christi, and just south of Houston, TX, in May 2005. The results of this paper show dependence on wind speed, rainrate, and polarization. They agree with numerous surface-based studies (single point measurements), using ocean platforms and wind-wave tanks, whose data were collected under similar conditions. For example, at rainrates less than 10 mm/hr, the relative change in surface roughness is seen to decrease as the wind magnitude increases from 5 to 7 m/s. Another consistent observation is that the vertical polarization NRCS shows less sensitivity to rainrate than does horizontal.**

***Index Terms*—Normalized radar cross section (NRCS), QuikSCAT/SeaWinds radar, rainrate over the oceans.**

I. Introduction

ON A GLOBAL scale, recent studies [14] have indicated that about 7% of the SeaWinds scatterometer (SWS) wind observations are affected by rain events. This paper seeks to contribute methods for obtaining more accurate scatterometer measurements in rain-affected regions. Important oceanographic advances and knowledge have been impeded by the presence of rain-contaminated wind vector estimates in the QuikSCAT (and in the SeaWinds/Midori-2) data products. These deficiencies systematically flag out low-pressure systems, which has a serious impact on estimates of ocean circulation, climatic studies, and operational applications. For example, the results obtained during studies of high-wavenumber surface wind forcing have been shown to contain significant biases and discrepancies [21]. Recent improvements in the rain flagging algorithm, now referred to as impact-based multidimensional histogram (IMUDH) [17], [24], are expected to reduce errors for future studies. This investigation uses the National Weather Service (NWS) Next Generation Weather Radar (NEXRAD) stations to provide quantitative estimates of precipitation distribution and intensity. Normalized radar cross section (NRCS) data from SWS and wind vector data products (available from JPL PO.DAAC) can be examined in the vicinity of the U.S. coastline (Gulf of Mexico, and from Florida up to New England) wherein National Oceanic and Atmospheric Administration (NOAA) and other buoys and numerous NEXRAD [9], [18] stations can provide near simultaneous, collocated surface, and near surface observations for actual winds and rain.

A unique method has been developed to utilize the volumetric scans of the S-Band NEXRAD radar (which has high spatial resolution; 1 km in range and 1° azimuth) to model the 3-D K_u-band reflectivity of the volume of precipitation that the scatterometer beam passes through as it samples the sea surface. This enables the correction to the measured NRCS for the effects of rain attenuation and rain volume backscatter. The removal of these effects leaves the total contribution of the sea surface; both the wind driven and rain-impact roughness terms. This paper is providing knowledge about the relative influences and contributions of these three mechanisms to the satellite measured NRCS at different wind speeds, rainrates, and polarizations.

Previous publications [10], [11] that addressed the effect of rain on QuikSCAT have employed data sets from multiple satellites that are not closely coincident or collocated. Their comparisons produce results that have plausible properties in the mean, but these also display considerable scatter. This is due to the limited resolution and accuracy resulting from time and spatial separations. Their use of integrated units of precipitation such as "km mm/hr" is based on near-nadir TRMM observations and the associated attenuation properties. This means that direct comparisons with this paper are of limited utility, since the impact roughness NRCS obviously depends on the liquid at lower altitudes. In this paper, by focusing on specific events with high resolution for space, time, and rain intensity, we see significant variations in the splash NRCS associated with the parameters of the radar configuration. Some of this is due to polarization and azimuth angle (relative to the wind direction).

Manuscript received September 22, 2007; revised April 11, 2008. Current version published October 1, 2008. This work was supported by the Physical Oceanography Program of the National Aeronautics and Space Administration (NASA) through Grants to Hofstra University and the Center for Ocean-Atmospheric Prediction Studies, Florida State University (through support by the NASA OVWST Project and the NASA/OSU SeaWinds Project).

D. E. Weissman is with the Department of Engineering Hofstra University, Hempstead, NY 11549 USA (e-mail: eggdew@hofstra.edu).

M. A. Bourassa is with Center for Ocean-Atmospheric Prediction Studies, Florida State University, Tallahassee, FL 32306-2840 USA.

Color versions of one or more of the figures in this paper are available online at http://ieeexplore.ieee.org.

Digital Object Identifier 10.1109/TGRS.2008.2001032

Natural rain events have the property that they are strongly inhomogeneous beyond distances of a few kilometers. The fact that rain cells typically have uniform intensities across horizontal dimensions of 2 to 2.5 km (covering only a few percent of the scatterometer NRCS footprint) means that innovative approaches need to be developed that can model the effect of these small rain cells on the 25×37 km^2 NRCS spatial measurement [12], [15]. By reconstructing a 3-D model of the precipitation and rain K_u-band reflectivity within a scatterometer beam, techniques were developed for removing this electromagnetic contribution to each NRCS measurement. The initial phase of this project produced techniques for modeling the volume backscatter and attenuation. These results are used (see Appendix) to estimate the influence of the remaining electromagnetic process that affects the scatterometer NRCS measurement; the rain impact "splash" roughness and its relative NRCS as a function of wind speed, rainrate, polarization, and relative azimuth angle.

II. Approach

The initial work created effective methods for using NEXRAD measurements at S-band to model the K_u-band volume reflectivity and attenuation for each scatterometer radar beam. The next step is to develop a model function for the rain-impact NRCS relative to the wind-only NRCS. This model function will depend on wind speed and rainrate. Experimental work by Braun and Gade [3], and Contreras *et al.* [5] and Contreras and Plant [6] have shown how the reflections from the rain-impact roughness depend on the incidence and electromagnetic polarization, as well as the atmospheric conditions. Other significant work has been done by Bliven and Giovanangeli [2] and Craeye [7]. Surface-based measurements involve either wavetanks, towers, or stationary ships. Only ocean-based observations can replicate the raindrop size distributions that occur in the atmosphere under the variety of stratiform and convective atmospheric conditions. With respect to the rain-impact roughness measurement, it is not yet clear what differences may exist between point measurements (from towers and ships) in which the illuminated area has uniform wind and rain conditions and satellite-based observations wherein the radar-illuminated region is nonuniform with respect to winds, waves, and rain.

For this paper, it was necessary to create collocated and coincident observations of the QuikSCAT NRCS that spans a wide swath of precipitation with high-resolution NEXRAD measurements of the 3-D reflectivity within the scatterometer beam. The significant difference between this measurement configuration and the surface-based techniques is that all these measurements are virtually coincident, and yet span a wide variation of rain intensity conditions across hundreds of kilometers. Furthermore, when the NRCS for wind driven roughness alone is to be estimated, it is only necessary to examine data from outside (but nearby) the rain limits. This would be an area where no rain reflectivity is detected (usually about 50 km away) and is assumed to have a similar mean wind to what exists under the rain. In addition, the ocean regions selected in this paper contain NOAA National Data Buoy Center (NDBC) buoys which can verify these inferences since their wind estimates are usually taken within a 100 km of the precipitation region. This coincident wind information is an advantage over satellite-based techniques [11] which used interpolated 6-h-spaced NCEP winds across a 2.5° grid, as input to a scatterometer model function. It is critically important to have near-simultaneous wind-driven NRCS values within 100 km of these rain observations, otherwise the data analysis could contain uncertainties of 2–3 dB which would weaken the results and diminish its utility.

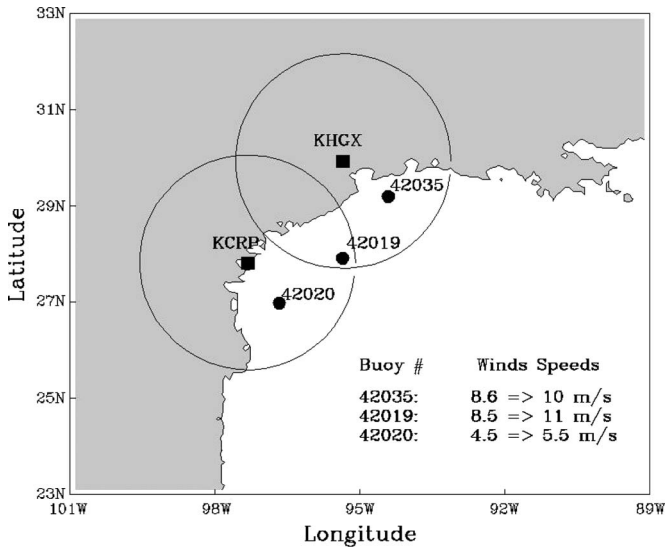

Fig. 1. Map of the Texas coastline in the Gulf of Mexico indicating the locations of the NWS NEXRAD stations at Houston (KHGX) and Corpus Christi (KCRP) and the NOAA-NDBC buoys. Also indicated are the wind speed ranges at the time (12 Z) of the QuikSCAT overpass at the respective buoys. The winds directions relative to north (oceanographic convention) are the following: buoy $\#42035 = 156°$; buoy $\#42019 = 190°$ and buoy $\#42020 = 129°$.

The NASA Jet Propulsion Laboratory maintains the data archives of QuikSCAT observations (since 1999). The NWS has continuous archives of NEXRAD data at all of its stations, so there are an abundance of measured events with desirable conditions of wind speed and precipitation. An optimum location for study is the section of the Gulf of Mexico just south of the Texas border, between Houston and Corpus Christi. NEXRAD stations are at each of these cities, and there are three NOAA-NDBC buoys in the region between them. Fig. 1 shows a map with the location of the buoys and NEXRAD stations in the region that includes Houston and Corpus Christi, and it lists the buoy winds at the time of a QuikSCAT observation that is of interest.

A. NEXRAD Instrument and Data Characteristics

The NWS operates this network of ground-based radar (3 GHz) stations, many of which were intentionally positioned close to the coastlines to provide high-resolution storm warnings for public safety. Their official designation is the Weather Surveillance Radar—1988 Doppler (WSR-88D) [8]. These were developed from a multiagency "Next Generation Weather Radar" program, hence the commonly used

"NEXRAD" acronym. There are 19 near the coasts of the U.S. covering the entire eastern seaboard and the Gulf of Mexico. All their Level-II data and software is publically available. Each data file contains dozens of analysis products, however only the reflectivity product is used here. It enables examination of rain magnitude (the reflectivity, "Z") and structure, in a spherical coordinate system, across the wide arc of beam coverage (maximum range $= 450$ km and elevation limited to 8 km, for this paper). Their volume coverage of the radar beam takes approximately 6 min to complete; therefore, their data files can provide conditions within the scatterometer beam with less than a 3-min time differential. The spatial resolution of the "Z" values is 1 km in range and 1° in azimuth. This data is converted into a 3-D matrix representing a volume with Cartesian coordinates. The interpolations used here result in a 2-km horizontal grid spacing in all directions, up to 250 km from each radar, and an altitude of 8 km with vertical steps of 0.5 km.

B. Electromagnetic Model of the Sigma0 Correction

The S-band (3 GHz) values need to be converted to $\mathrm{K_u}$-band reflectivity and attenuation. This has been accomplished by using fundamental data on the backscattering and extinction coefficients of raindrops, through a collaboration with Dr. Stephen Durden [13]. A mathematical model has been developed which represents the principal electromagnetic mechanisms of rain; attenuation and volume scattering, using the polarization and illumination details for the SWS. Its properties are different from most of the literature in radar meteorology concerned with S-band measurements and applications. The dual polarized $\mathrm{K_u}$-band radar on SWS requires a different method of electromagnetic calculations. The three commonly used assumptions for S-band, namely spherical raindrops, Rayleigh electromagnetic scattering, and the Marshall–Palmer raindrop size distribution, are not suitable for the $\mathrm{K_u}$-band radar beam with these incidence angles and in all geographic regions. Like many in the research community who use radar at this frequency, we favor the more elaborate dropsize distributions (DSDs) of Haddad *et al.* [16]. Electromagnetic backscattering (their individual radar cross sections) and extinction coefficients for raindrops were calculated for $\mathrm{K_u}$-band as a function of their size, shapes (oblateness), and incidence angle. This function of raindrop size is combined with the DSD to calculate the "equivalent radar reflectivity factor" which only reduces to the commonly used reflectivity factor "Z" for spherical raindrops when the Rayleigh approximation is valid [20, Ch. 2]. This rigorous approach leads to polarization differences in the volume reflectivity.

The critical step in modeling this reflectivity is the choice among the wide range of parameters that could specify the DSD, including the assumptions about stratiform and convective rainfall. Of special interest here is that Haddad *et al.* [16] produced a thorough analysis, sets of parameters and consequent k–Z and Z–R relationships for a wide range of frequencies. The choice between stratiform versus convective drop-size parameters leads to very different outcomes for the reflective factor and attenuation [1].

It is well known that rain DSD varies seasonally and regionally. Whether a particular observation within an event is dominated by stratiform or convective conditions depends on the local conditions, and these can vary over areas of 50 km or more. It is likely that the event shown in Fig. 2 includes both stratiform and convective conditions. Schumacher and Houze [23] point out that stratiform conditions apply in rain rates that are less than 3 mm/hr, in the $\pm 20^\circ$ latitude range observed by TRMM. It should be noted that this study is at a location just above 25° N. It is not clear how homogeneous a given scatterometer footprint is with respect to these two categories. Since no additional data is available to influence our opinion about these properties we needed to rely on the characteristics of the results we obtain when we tested both possible assumptions. An early phase of this investigation made the assumption of stratiform rain for both the volume backscatter and attenuation calculations. We found this to be problematic for rainrates above 2 mm/hr because there appeared to be excess volume backscatter and attenuation. We found little difference in the consequences when the rainrates were less than 2 mm/hr. Therefore the choice was made to use the convective-based parameters listed in Haddad's tables. The consequences of this selection will be discussed further in connection with the final results in Section IV.

Column integration (along the proper angle for each incident beam) then produces the needed correction terms. The rain volume within the scatterometer beam is modeled using $5 \times 5 \times 2$ km^3 (elevation) cells. These typically display widely different reflectivities within one footprint. These discrete reflectivity and attenuation steps, from the 48 subcells at each of the four altitudes, are combined and used to process the measured NRCS to model a single QuikSCAT corrected Sigma0 measurement. The attenuation values are calculated from the $\mathrm{K_u}$-band reflectivity estimates using relationships developed by Haddad *et al.* [16], with parameters related to a convective rain event. For the attenuation calculation, no differential for electromagnetic polarization is assumed.

The calculation procedure is presented in the Appendix. This is a model for the total measured Sigma0 which combines the rain contributions (atmospheric) with the primary wind driven roughness plus the rain-impact "splash" contribution. This equation makes it clear which terms have to be measured or estimated in order to extract the best possible estimate of the wind driven roughness term (σ_{wdx}) and the rain driven roughness term (σ_{rnx}) for each respective polarization ($\mathrm{x} =$ either "v" or "h"). An explanation of the use of this equation will be presented below, in conjunction with the 3-D precipitation model.

C. Modeling the High-Resolution Precipitation Structure and NRCS Correction

To illustrate the conversion of the NEXRAD reflectivity data into a 3-D $\mathrm{K_u}$-band reflectivity Cartesian volume, a SeaWinds event is selected. This observation employed the NEXRAD level II data from the Melbourne, FL, station (KMLB) on July 24, 2003, at a time that was within 3 min of the satellite scatterometer overpass. The NEXRAD data is shown in Fig. 2

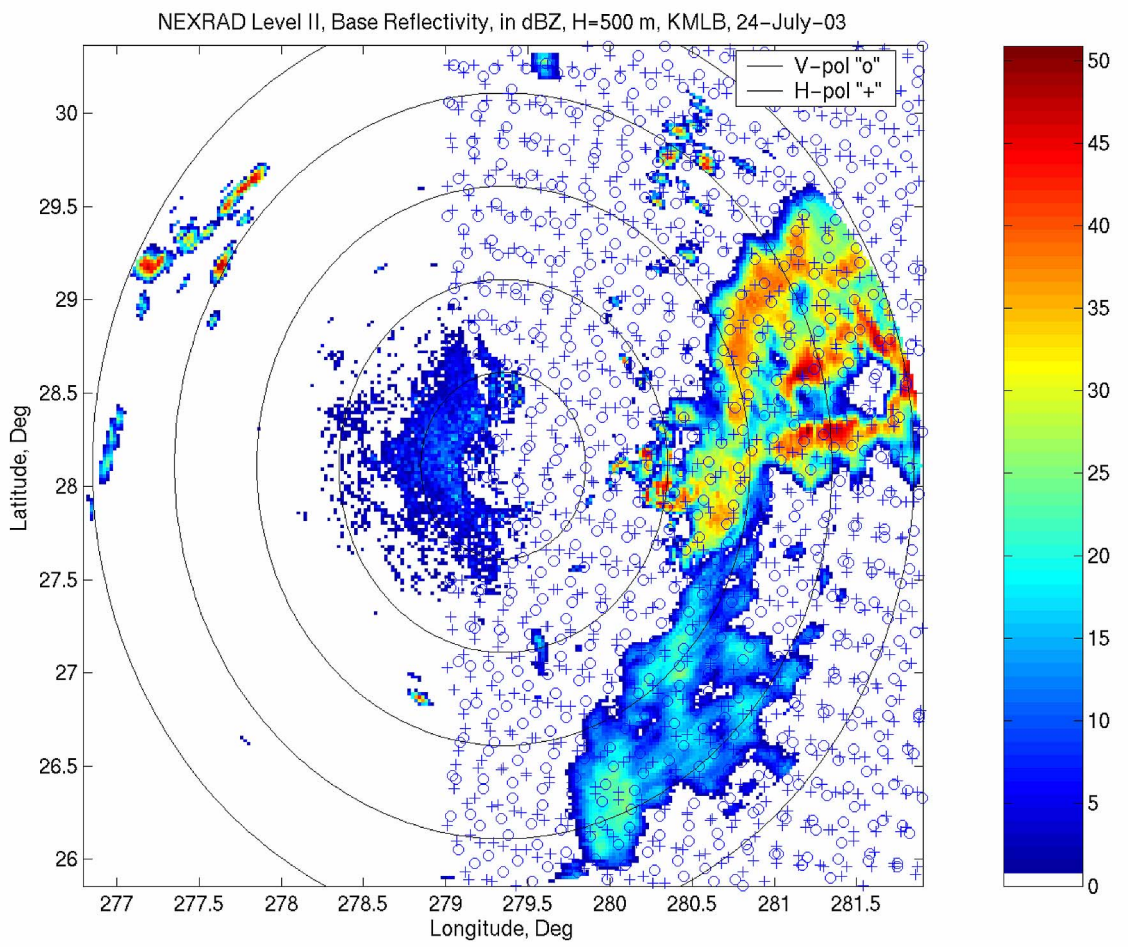

Fig. 2. Horizontal slice of NEXRAD reflectivity (in dBZ) at t $= 16:00$ Z, (the time of the SWS overpass) from the KMLB radar. The location of the centers of the SCAT cells (from the L2A product) are plotted and identified as either H or V polarization. Land boundaries not shown. The ellipses represent 50-km distance increment circles, distorted due to the Lat–Long axis.

with color coding based on the logarithm of the reflectivity (in decibels relative to a standard reference value, dBZ). The maximum reflectivity given in the colorbar, 50 dBZ, is approximately equivalent to a surface rainrate of 60 mm/hr. It is the S-band base reflectivity extrapolated down to an altitude of 500 m, with a horizontal resolution of 2 km (using the first Cartesian volume derived from the spherical coordinate-based measurements). Also shown in this graph are the points representing the locations of the centers of the scatterometer observation areas (for Advanced Earth Observing Satellite-II orbit #3172), where the H-pol and V-pol cells are separately identified.

As a compromise between the 2-km horizontal resolution available from the NEXRAD at these distances and the goal of less computational complexity, a $5 \times 5 \times 2$ km grid was selected to represent the reflectivity field at each of four elevations. Fig. 3 shows a 2-D view of the individual reflectivity cell locations within the 3-dB spaces contours of the antenna illumination ("egg") patterns [19]. The antenna beam axis is centered in the 8×6 array, and each elliptical contour represents a 3-dB drop in received (two-way) amplitude. Therefore, many of the 5-km grid cells on the outer edges of this rectangular area may make a minor contribution to the received signal; about 20 of the 48 cells lie within the 3-dB contour. However, this will depend on the local reflectivity, as shown in the highly variable intensity structure presented in Fig. 5. Each QuikSCAT cell has its NEXRAD volume correctly rotated and aligned according to the scatterometer azimuth look direction, and incidence angle of the radar beam.

A critical fact of the antenna illumination of rain is that the steep incidence angles lead to horizontal displacements of observations at different height. A side view of the slanted parallelopiped, which constitutes the rain volume from which volume scattering and attenuation must be computed, is shown in Fig. 4. Each Sigma0 observation is processed with volume reflectivity and attenuation from its aligned NEXRAD volume.

There are 196 separate cells that constitute one of the "beam volumes" shown in Figs. 3 and 4. Samples of the distribution of reflectivity (in dBZ) among these positions is shown for a single QuikSCAT observation in Fig. 5. This data point was located at Lat $= 29^\circ$ and Long $= 281^\circ$ in Fig. 2. The structure of the reflective volume has four stratified layers, corresponding to the layout shown in Figs. 3 and 4. This model represents a surface area coverage of 30×40 km^2. At the lowest layer, variations in reflectivity of 10 dBZ are shown within the "egg" 3-dB contour of Fig. 3. At the 3-km elevation layer, 15-dBZ variations are noted. The correction process to estimate "σ_{wdx}" modeled in the Appendix involves integrating the volume backscatter,

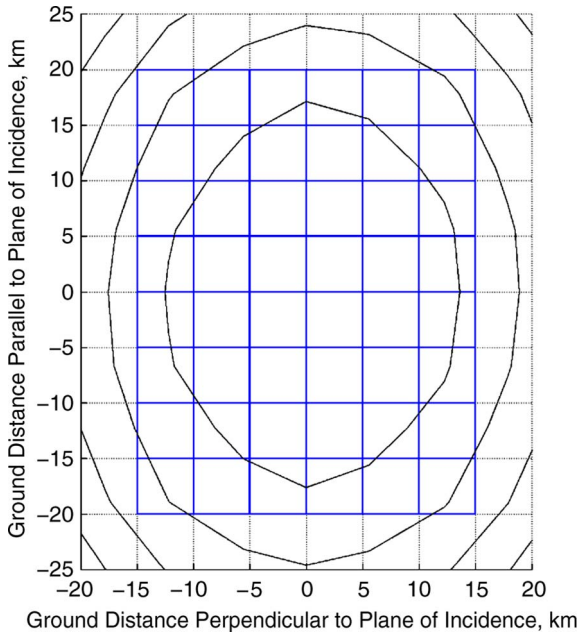

Fig. 3. Subdivision of scatterometer antenna illumination of rain into grid boxes which represent uniform NEXRAD reflectivity cells (5×5 km^2, by 2 km high), at one of four elevation levels. Elliptical contours are 3 dB (decreasing) increments of the "egg" antenna pattern coverage, characteristic of the SeaWinds antenna.

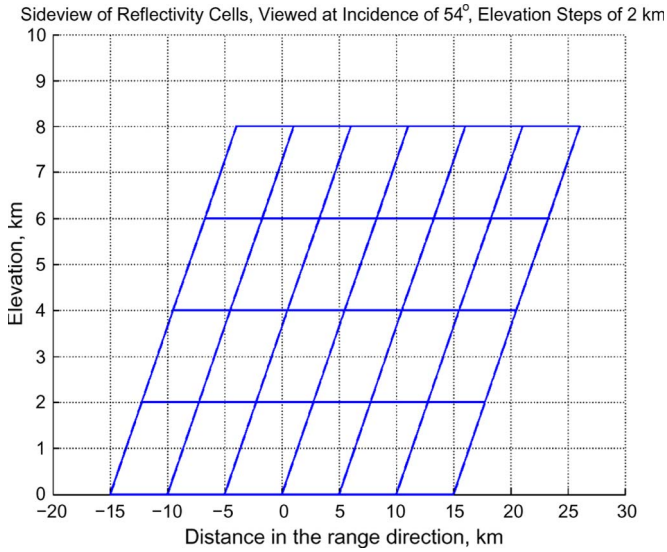

Fig. 4. Sideview of reflectivity cells within V-pol incident beam. Note displacement of upper level cells relative to lower cell locations.

"$\sigma_{\rm ox}$," and attenuation "$\alpha_{\rm x}$" along each of the 48 separate reflectivity beams shown in Fig. 5.

D. Estimation of the Relative Change in NRCS

The model used to represent the measured NRCS in the presence of rain is stated in (1), where $\sigma_{\rm ax}$ is either $\sigma_{\rm av}$ or $\sigma_{\rm ah}$ depending on the polarization. It is the sum of two separate terms; the volume backscatter plus the surface return which is affect by two-way attenuation. The preceding discussion indicates the geometric aspects of how the volume backscatter and attenuation are computed for each QuikSCAT cell. Their substitution in (1) enables the calculation of the total surface return $\sigma_{\rm wdx} + \sigma_{\rm rnx}$, which is the sum of the wind-driven surface NRCS which would be observed in the absence of rain plus the change incurred by rain impacts. As indicated in (2), dividing this by $\sigma_{\rm wdx}$, which can be estimated with NRCS data points measured just outside the rain area (at the same polarization azimuth angle and wind regime), gives the relative change resulting from the rain impacts $\sigma_{\rm rn0}$. This paper provides a case study of how this ratio $\sigma_{\rm rn0}$ can be modeled as a function of wind speed and rainrate at each polarization.

III. Description of Observations

The region in the Gulf of Mexico just south of Houston is an attractive area for our comparisons because of the presence of two NEXRAD stations, KHGX (Houston) and KCRP (Corpus Christi), both close to the coastlines (see Fig. 1). The circles drawn around the stations in this figure define ranges of 250 km from each radar. Two buoys lie within each of the circles. On May 30, 2005, a broad and intense rain event covered the Texas Gulf coast from Corpus Christy to across the Louisiana border. Fig. 6 shows the S-band reflectivity from KCRP NEXRAD at the time of the QuikSCAT overpass, about $\rm t = 12:00$ Z. Its interesting features show it contained large areas of intense rain (> 35 dBZ) and gradients of varying intensity toward each of the NEXRAD's. The swath of SWS on QuikSCAT illuminated a region large enough to include all areas of interest.

Numerous QuikSCAT observations (Fig. 7) lie within the KCRP observation region. The centers of the scatterometer footprints are plotted with their corresponding polarization labels, and those points for which the volume NRCS exceeded the measured value are labeled in red and are excluded from the analysis. In an attempt to create spatial regions in which as many of the radar parameters as possible are relatively constant, two adjacent rectangular areas (about 1° in size) were defined as "BOX 1" and "BOX 2." Surface wind measurements [nearly simultaneous with the QuikSCAT overpass (see Fig. 1)] indicated that the mean wind speeds were different in each of these. In BOX 1, the mean wind is estimated to be 7 m/s in the direction of 190°. A lower wind of 5.3 m/s, with a 129° direction, was measured by buoy #42020 in BOX 2, in its northwest section. The QuikSCAT observations in each box can be segregated into just two azimuth look directions (having variations within a 30° range). Their values, defined as being measured clockwise from north (oceanographic convention), will be specified below.

In order to estimate the rainrate at the surface, the NEXRAD reflectivity in each cell across the lowest levels of the 3-D array [corresponding to an elevation of 1-km (see Fig. 4)] is converted to rainrate, then horizontally averaged across the size of a QuikSCAT cell, to produce "R," in millimeters per hour. The color-coded circles in Fig. 8 indicate this rainrate magnitude but plotted at the centers of each of the scatterometer cells. The size of these plotted circles are arbitrary and are not intended to model the relative size 25×37 km^2 antenna footprint of each QuikSCAT cell. Then, the variations in NRCS for its location at the points in each box can be studied as a function of this rainrate, and further separated into nearly

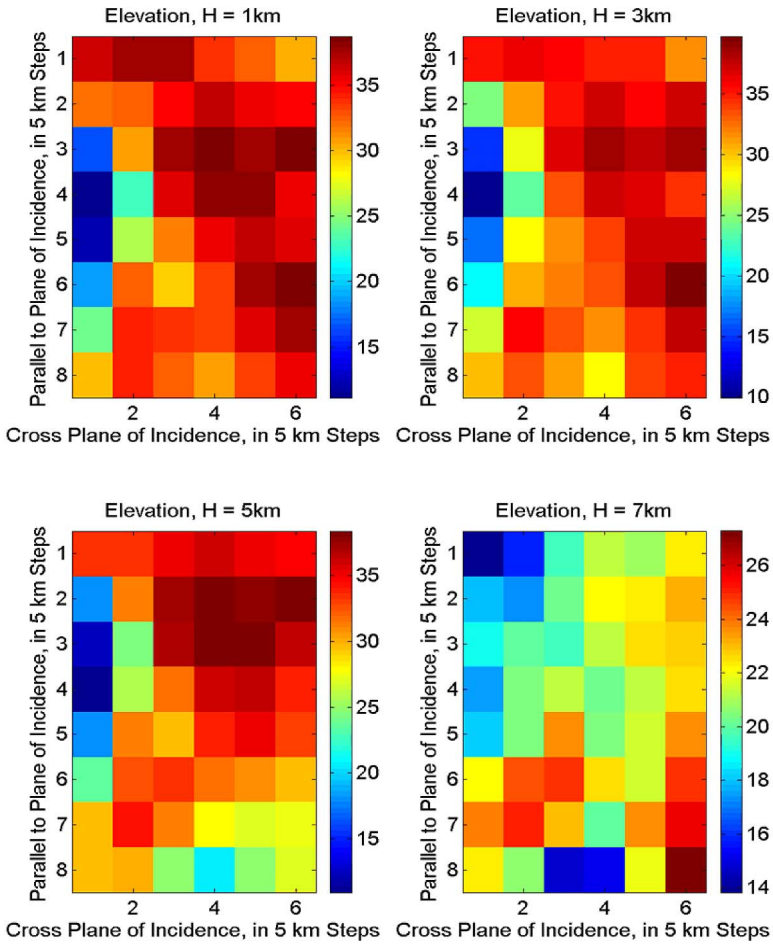

Fig. 5. Five-kilometer reflectivity cells within each of four layers of that constitute the NEXRAD volume reflectivity model within one SCAT measurement, from the July 24 overpass (Fig. 2). The cell location is Lat $= 29°$, Long $= 281°$. This illustrates the strong variability within a QuikSCAT cell.

constant azimuth angles and wind speed groups. It is worth emphasizing, when noting the close locations of the V-pol and H-pol data points in Fig. 7, that they are effectively collocated. Therefore, they are observing virtually the same wind, wave, and rain-filled atmosphere when they are identified with the same surface rainrate value from Fig. 8.

IV. Surface NRCS and Relative Rain-Impact Roughness

One such region, BOX 1, ranges from Long $= 263.5°$ to $264.5°$ and Lat $= 27°$ to $28.25°$. The wind speed here is in the 6 to 8 m/s range. There are 164 scatterometer NRCS observation cells, extracted from the PO.DAAC Level 2A data product [17], which lie in this region; 93 are H-pol and 71 are V-pol. These are then separated into two groups, by azimuth angle look direction. Referring to the Appendix, the measured values are either $\sigma_{\rm av}$ or $\sigma_{\rm ah}$ at each respective polarization, and at that specific azimuth angle. In Fig. 9 (upper plot), the measured H-pol NRCS, at one cluster of azimuth angles, is plotted versus the corresponding rainrates from Fig. 8, using the "+" symbols. All NRCS data plotted herein using the "+" symbol will represent original measurements from the L2A data files, with no alteration. The azimuth angle is arbitrarily labeled as #1, and they span a $10°$ range centered about $175°$. The NRCS values observed in cells where the mean rainrate is less than 0.1 mm/hr (a higher threshold of 0.3 mm/hr was used for the V-pol groups) are averaged and serve as a reference in which the "no-rain" and wind only value can be estimated. In the Appendix, this quantity is defined as $\sigma_{\rm wdx}$, for the respective polarization group in that box. Starting at a mean rainrate of 1 mm/hr, there is a steady increase in this measured NRCS. At the highest rainrate close to 10 mm/hr, the typical change is about 6 dB before any corrections are made.

In order to remove the effect of rain volume backscatter and atmospheric attenuation for each scatterometer measurement, the method of the Appendix is followed. By removing the atmospheric volume reflectivity part of the NRCS and correcting for the two-way attenuation, the "corrected" NRCS is plotted as the colored square symbols versus rainrate. This now only represents the wind driven plus the rain-roughened surface impact NRCS; $\sigma_{\rm wdh} + \sigma_{\rm rnh}$, and this is referred to as the "corrected NRCS" at the surface. At 2 mm/hr and below, there is negligible difference between the measured and corrected values. Above this level, clear differences indicate that the corrected value can be smaller or larger than the measured value, depending on whether the volume correction or two-way attenuation is dominant. As discussed in Section II-B, the

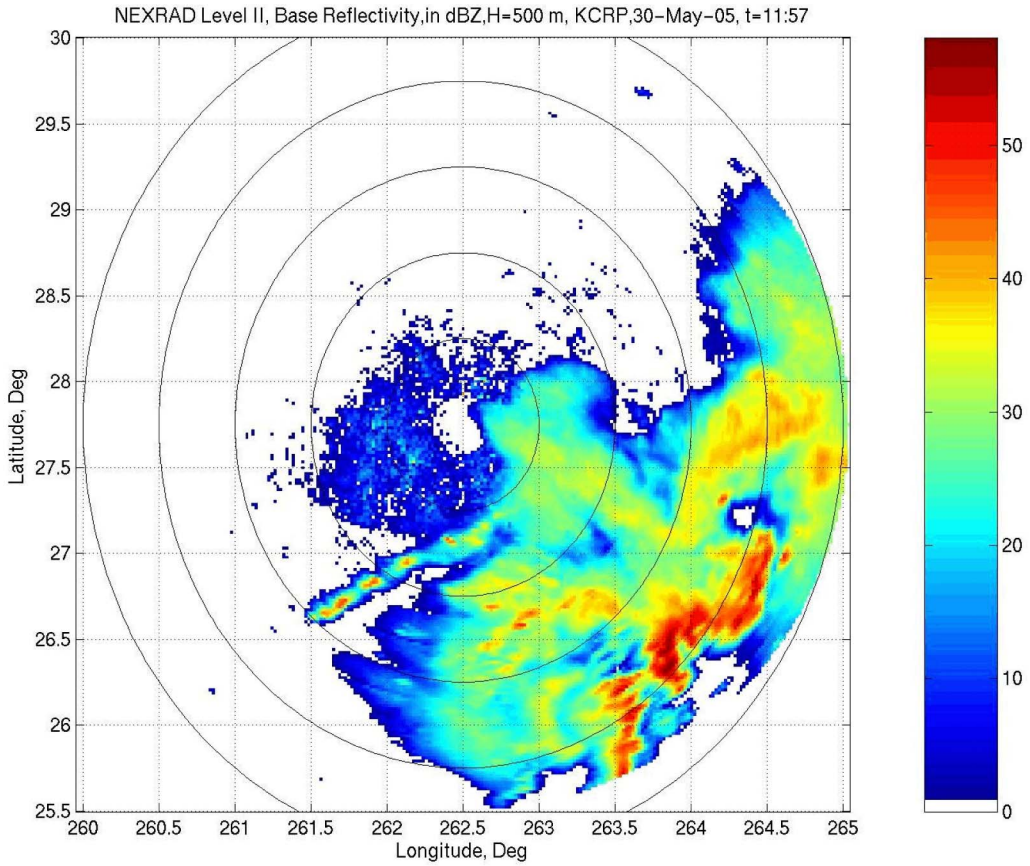

Fig. 6. Interpolated S-band reflectivity at altitude of 500-m elevation, in dBZ (40 dBZ equivalent to 20 mm/hr rainfall), within a range limit of 250 km from the KCRP NEXRAD station.

results here are very sensitive to the parameter in the DSD that determines a convective or stratiform rain model. Our choice was "convective" which was partially influenced by our consideration of the stratiform model, which led to problematic results.

The NRCS values in the very light rain areas (< 0.1 mm/hr) give us a mean value of about -19 dB to normalize all the corrected NRCS. The plotted points in the lower half of this figure are the ratio (in decibels) of the wind-plus-rain impact NRCS to the "no-rain" NRCS at the same conditions of wind speed, polarization, and azimuth angle look. This is defined as σ_{rn0} in the Appendix [(2)]. The wind magnitude in this area is estimated to be in the range of 6–8 m/s. The results show a steady increase in the impact NRCS, with a nominal value of 7 dB at a rainrate of 10 mm/hr. Fig. 10 shows a similar plot but for the observations at the second azimuth angle of 337°, labeled as #2. For the areas where the rainrate is negligible (less than 0.1 mm/hr), the typical σ_{wdh} values are about 2 to 3 dB less than for azimuth #1. This is to be expected since in rain-free areas, variations with azimuth angle are a fundamental property in how scatterometers can be used to determine direction. This difference persists up to rainrates of 1 mm/hr and higher. However, in the more intense rain area, the observed and corrected values are closer for both azimuth angles. Therefore, for azimuth #2, the incremental increase of σ_{rn0} at the 10 mm/hr rainrate shows a slightly higher net change of about 9 dB. The highest rainrates available in Box #1 were 12 mm/hr, but higher intensities were seen in the Box #2 analysis.

After examining these preliminary results, it is advisable to consider the variability of the data and the calculated results. The efforts at parameter separation and grouping seek to limit the variability in the measured and corrected NRCS to only that caused by sea surface and atmospheric rain inhomogeneity, and not that induced by the radar parameters. The measured NRCS in the upper graph of Fig. 9, for rainrates below 0.1 mm/hr, illustrates this expected variability. The mean value is -19.4 dB with a standard deviation of 1.3 dB. Therefore, it is reasonable to infer that the vast majority of natural variability in our NRCS data will be contained within a 3-dB range. Allowing for the strong inhomogeneities in rain intensities and structure pointed out in Figs. 5 and 6, we would expect larger variability at the more intense rainrates, with occasional "outliers." This is shown in the additional results in Fig. 9. In Fig. 10, for Azim, #2, the mean measured NRCS below 0.1 mm/hr is -22 dB with a standard deviation of 1.3 dB, and all its other results are consistent with our expectations from Fig. 9.

The simultaneous and collocated V-pol data in BOX 1 shows some distinct differences compared to H-pol. In Figs. 11 and 12 (upper plots), there are slightly higher surface V-pol NRCS for the very low rain conditions compared to H-pol at the same azimuth angles. The mean "no-rain" NRCS is -18 and -19 dB, respectively, and their variability is similar to H-pol values. This finding is consistent with the scatterometer model

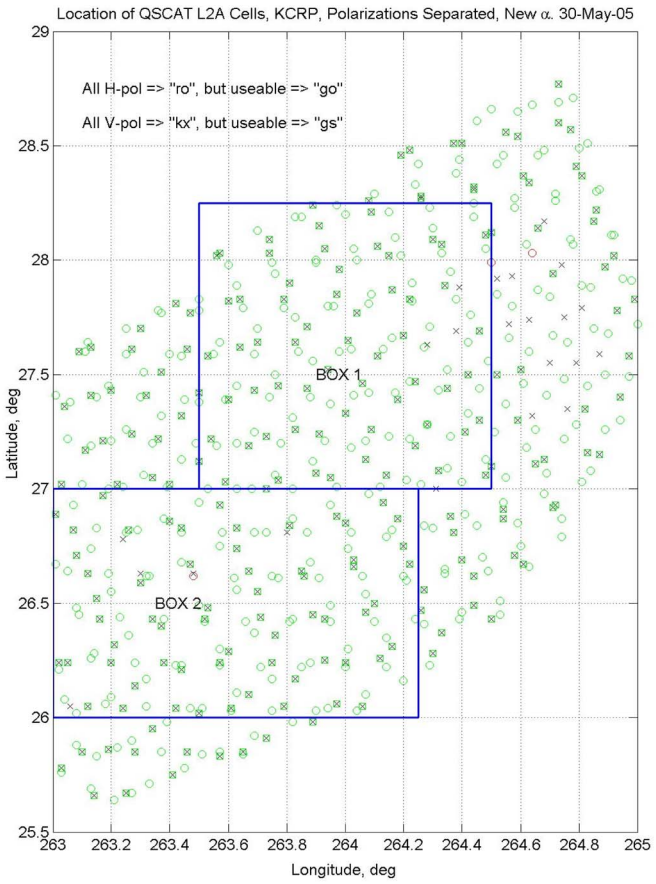

Fig. 7. Locations of the QuikSCAT L2A cells within a rain event near the KCRP NEXRAD. The usable H-pol and V-pol points are designated with green circles or green squares, respectively. QuikSCAT cell size typically 25×37 km^2.

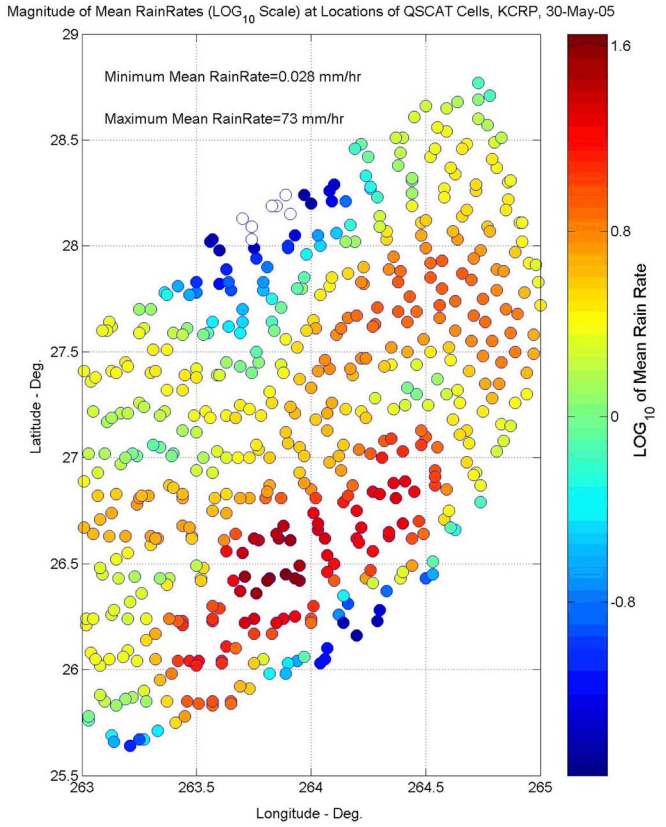

Fig. 8. Location of the QuikSCAT cells (both H-pol and V-pol) with the mean rainrate magnitude within each cell, as displayed with a logarithmic color scale.

function and measurements by Contreras *et al.* [5]. However, at the same rain locations and azimuth look directions that led to an increase in the H-pol NRCS by 2 dB, this measured V-pol collection only increases by about 2 to 3 dB. This difference could only partly be explained by the differential reflectivity of nonspherical raindrops at $\mathrm{K_u}$-band. which was also detected in a previous study [26]. These values are normally on the order of 1 dB at these rainrates [1].

In those V-pol cells in which the mean rainrate is 4 mm/hr and above, the corrected NRCS is seen to increase but by only a small amount, noticeably less than what the H-pol increase was. Also, we see a sizeable (but minority) population of corrected NRCS values $(\sigma_{\mathrm{wdv}} + \sigma_{\mathrm{rnv}})$ that are lower than the no-rain cases. Considering that there is a 5-dB spread in the values for rainrates between 4 and 9 mm/hr, the V-pol data alone provide insufficient evidence to identify a physical basis for this effect beyond the inherent variability noted earlier. However, the difference from H-pol suggests that the rain-roughened surface has distinctly different properties for V-pol, at this combination or rainrate and wind speed. To further support this conjecture, it should be kept in mind that these separate polarization measurements are closely located in space and will therefore be affected by very similar atmospheric conditions. In contrast, the results to be presented for BOX 2 which has a lower wind speed (in the 4 to 6 m/s range), show these two polarizations to have very similar behavior.

The wind and rain conditions in the region labeled BOX 2 are noticeably different. The wind speeds are estimated to be in the range from 4 to 6 m/s. There are several scatterometer cells in areas where rainrates are up to 60 mm/hr. However, the results for H-pol for both azimuth angles in Figs. 13 and 14 are very similar. These azimuth angles are 180° (#1) and 332° (#2). Both figures indicate that the H-pol measurements display lower NRCS in the very low rainrate areas than were seen in BOX 1. However, when we examine the cells where the rainrates are in the range from 5 to 10 mm/hr there is little difference between these measured NRCS from those in BOX 1. This indicates that the combine atmospheric and rain-affected surface effects dominate the observation at this rain intensity, and wind speed. Looking at the lower plots in each figure, we can see that for rainrates between 2 to 5 mm/hr, the rain roughening has a relative strong affect on the surface NRCS.

It is encouraging that the V-pol measurements in BOX 2 do not display any of the problematic features that were seen in BOX 1 (Figs. 11 and 12). Both V-pol azimuth angle sets (see Figs. 15 and 16) display very similar measured NRCS to each other. For rainrates above 5 mm/hr, the measured V-pol NRCS is indistinguishable from their H-pol counterparts. When we compare the final calculations of the relative changes in the surface NRCS for both polarizations, we find very similar behavior and magnitudes. While small differences are observed, these do not warrant a critical assessment because there were

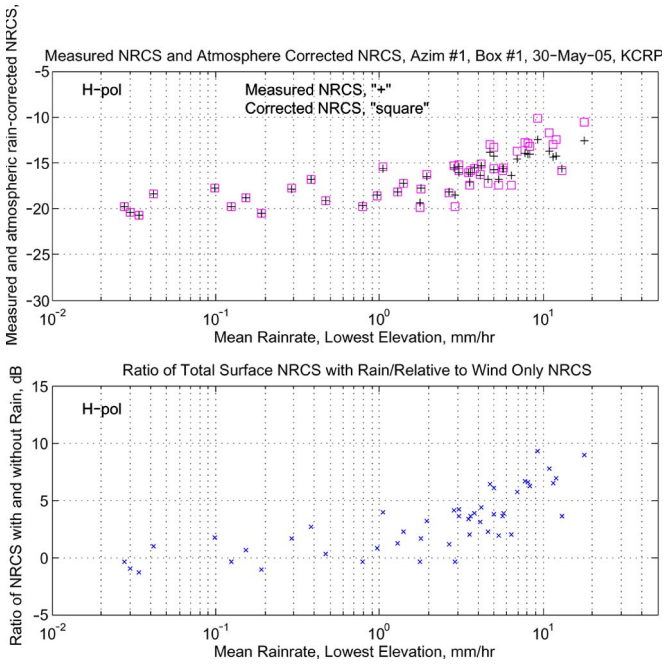

Fig. 9. H-pol data and calculations for Box #1, Azimuth Angle #1 (mean of 175°, relative to north), Upper plot: Uncorrected and corrected (for atmospheric rain) H-pol NRCS versus mean rainrate at each QuikSCAT cell. Lower Plot: Ratio of total surface NRCS to wind-driven NRCS versus rainrate. Mean wind is 7 m/s, toward 190°.

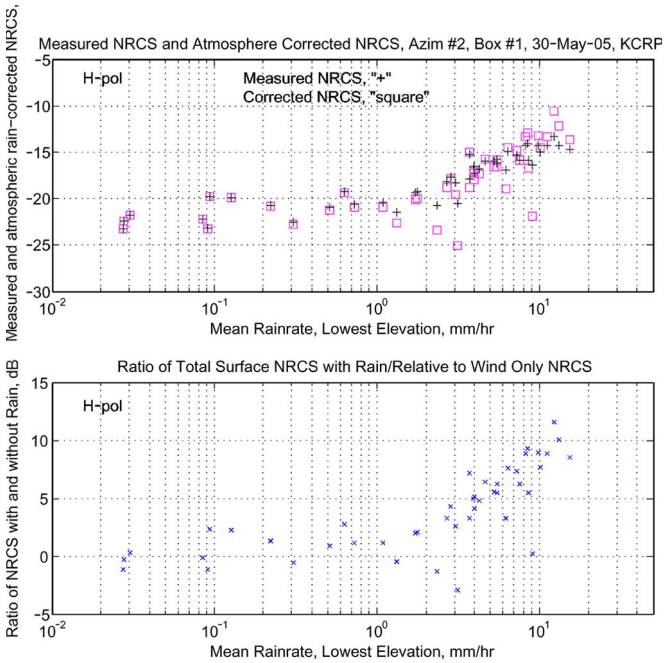

Fig. 10. H-pol data and calculations for Box #1, Azimuth Angle #2 (mean of 337°, relative to north), Upper plot: Uncorrected and corrected (for atmospheric rain) H-pol NRCS versus mean rainrate at each QuikSCAT cell. Lower Plot: Ratio of total surface NRCS to wind-driven NRCS versus rainrate. Mean wind is 7 m/s, toward 190°.

very few V-pol data points in BOX 2 that were in the "no-wind" area. Additional points here could easily affect the reference value of the NRCS. It is hoped that further studies will better define these roughness-enhancement functions under similar and higher wind conditions.

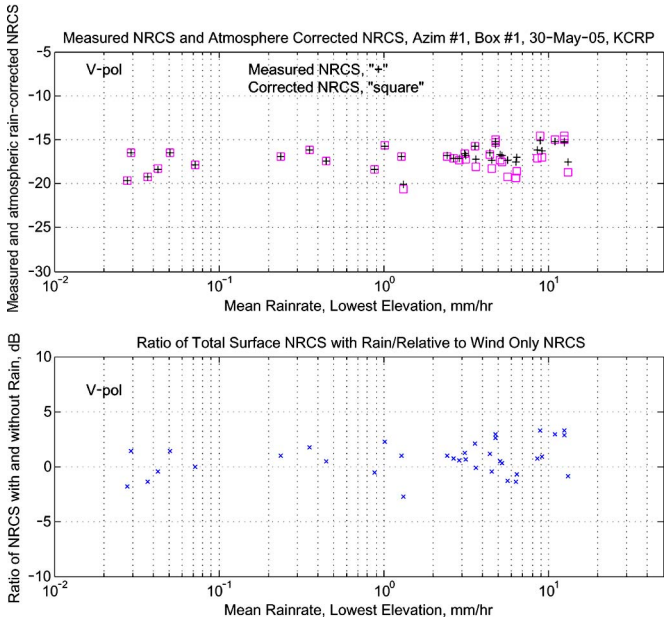

Fig. 11. V-pol data and calculations for Box #1, Azimuth Angle #1 (mean of 175°, relative to north), Upper plot: Uncorrected and corrected (for atmospheric rain) V-pol NRCS versus mean rainrate at each QuikSCAT cell. Lower Plot: Ratio of total surface NRCS to wind-driven NRCS versus rainrate. Mean wind is 7 m/s, toward 190°.

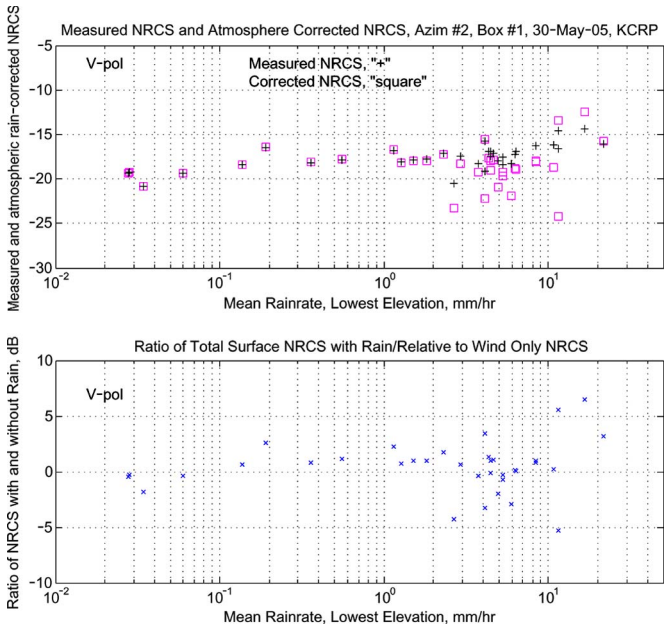

Fig. 12. V-pol data and calculations for Box #1, Azimuth Angle #2 (mean of 337°, relative to north), Upper plot: Uncorrected and corrected (for atmospheric rain) V-pol NRCS versus mean rainrate at each QuikSCAT cell. Lower Plot: Ratio of total surface NRCS to wind-driven NRCS versus rainrate. Mean wind is 7 m/s, toward 190°.

V. Summary and Discussion

This research program seeks to collect information equivalent to a model function that quantifies the relative change of the surface NRCS caused by rain, at any wind speed for each of the polarizations of QuikSCAT. One of many difficulties in this endeavor results from the relatively small scale of spatial

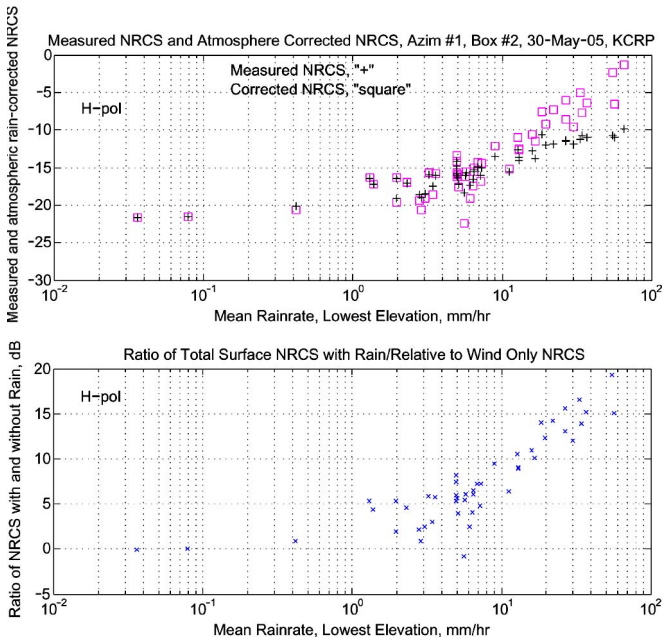

Fig. 13. H-pol data and calculations for Box #2, Azimuth Angle #1 (mean of 180°, relative to north), Upper plot: Uncorrected and corrected (for atmospheric rain) H-pol NRCS versus mean rainrate at each QuikSCAT cell. Lower Plot: Ratio of total surface NRCS to wind-driven NRCS versus rainrate. Mean wind is 5.3 m/s toward 129°.

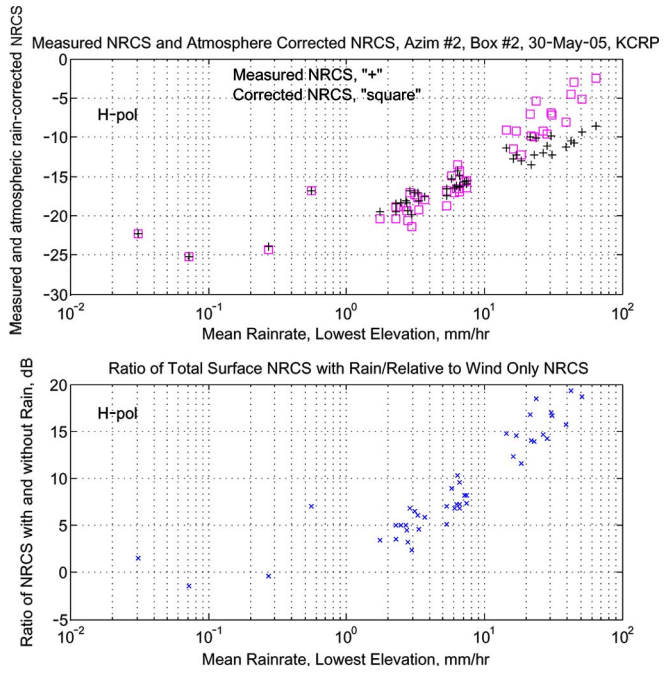

Fig. 14. H-pol data and calculations for Box #2, Azimuth Angle #2 (mean of 332°, relative to north), Upper plot: Uncorrected and corrected (for atmospheric rain) H-pol NRCS versus mean rainrate at each QuikSCAT cell. Lower Plot: Ratio of total surface NRCS to wind-driven NRCS versus rainrate. Mean wind is 5.3 m/s toward 129°.

inhomogeneity of the rain within the nominal 30-km-sized scatterometer footprint size. The unique contribution of this paper is to create a configuration in which the 3-D structure of atmospheric rain within the radar beam can be measured using the ground-based NEXRAD radar virtually simultaneously with the satellite observations. The resolution of this

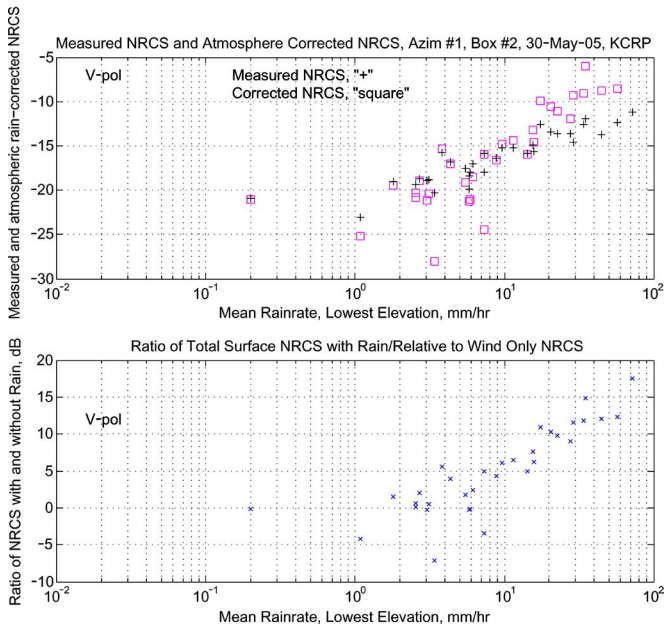

Fig. 15. V-pol data and calculations for Box #2, Azimuth Angle #1 (mean of 180°, relative to north), Upper plot: Uncorrected and corrected (for atmospheric rain) V-pol NRCS versus mean rainrate at each QuikSCAT cell. Lower Plot: Ratio of total surface NRCS to wind-driven NRCS versus rainrate. Mean wind is 5.3 m/s toward 129°.

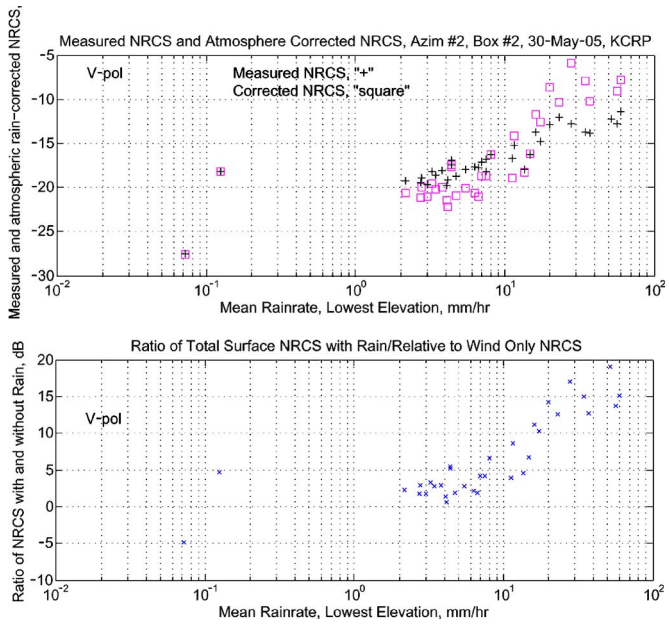

Fig. 16. V-pol data and calculations for Box #2, Azimuth Angle #2, (mean of 332°, relative to north) Upper plot: Uncorrected and corrected (for atmospheric rain) V-pol NRCS versus mean rainrate at each QuikSCAT cell. Lower Plot: Ratio of total surface NRCS to wind-driven NRCS versus rainrate. Mean wind is 5.3 m/s toward 129°.

S-band instrument is excellent, but it does have limitations in its vertical dimension. When observations are coordinated to be over ocean regions that contain nearby, multiple NDBC buoys to provide simultaneous surface winds, this assembly of resources constitutes conditions analogous to a "laboratory" although individual observations cannot be repeated. Considering the very extensive QuikSCAT and NEXRAD data archives, a specific region can be studied with many repetitions. The

approach presented in this paper uses a single weather event to illustrate this technique, the relevant data sets and the quality of the results.

The region of the Gulf of Mexico selected for this paper was advantageous since it contained two independent NEXRAD systems that provided complete coverage of the rain distribution during a QuikSCAT overpass. This configuration was supported by timely NOAA buoy wind measurements. The NCEP-based "model winds" that are provided as a QuikSCAT data product were also employed to obtain an overview of wind conditions across the region. Appreciable variations of wind magnitude were detected over spatial distances on the order of 100 km, and these were utilized in planning the analysis. It was decided that it would preferable to separate the radar measurements and model results into adjacent areas (Boxes #1 and #2) with different wind speeds. The overlap in the spatial coverage of the two NEXRAD radars (see Fig. 1) was used to test the method of 3-D modeling the atmospheric reflectivity factor which enabled the calculation of the volume radar cross section and attenuation for each scatterometer cell.

The quantitative assessment of the properties of the rain-impact roughness is based on the ratio of total surface NRCS relative to that in a close-by region where only the wind-driven NRCS is observable. A survey of the measurements and model calculations shown in Figs. 9 to 16 show distinct, resolvable features for the dependence on wind speed and azimuth look direction in addition to rainrate. In the winds speed range of 6 to 8 m/s that existed in box #1, the H-pol results (Figs. 9 and 10) display azimuthal differences for rainrates below 2 mm/hr where wind driven roughness is dominant, and behaves accordingly. The same property is shown for the V-pol data at the lower rainrates in Figs. 11 and 12 at the two different azimuth angles. At appreciable rainrates above 2 mm/hr, the character of the V-pol dependence on increasing rainrates is markedly different from that of H-pol. The latter dependence shown in Figs. 9 and 10 shows a steady distinctive increase up to about 15 mm/hr, indicating a relative change in roughness of 8 to 10 dB. However, the V-pol data in Figs. 11 and 12 show no such trend; only values mostly in the 1 to 3 dB range, with a several negative excursions in the NRCS ratios in the lower portions of these figures. There is no clear precedent in the literature for these negative values, but these are not the only anomalies. Even in the range from 5 to 10 mm/hr, very few of the measured and corrected NRCS rise more than 2 dB above the nominal "no-rain" values of -18 and -19 dB, respectively. It is difficult to identify any artifact of the correction calculations that would account for this wide extent of curious features. When glancing ahead to the results obtained in Box #2 at the lower winds, no similar problem exists for either the V-pol or H-pol results.

One basis for studying this anomaly further would be the generally accepted view that the electromagnetic scattering mechanisms for a rain-impacted surface is different for H-pol versus V-pol. There is evidence that V-pol backscatter is principally from the propagating ring waves generated by falling drops, and the H-pol backscatter is mainly associated with the nonpropagating crowns and stalks [3], [6]. However, little is known about the relative dependence of these distinct features in the presence of moderate to strong winds, when the wind-driven centimeter waves are growing in their amplitude and spatial extent, and complex long wave systems may exist. Hopefully, future research efforts will be directed at addressing this question.

It is worth exploring some related knowledge found in the literature to interpret the V-pol results in Box #1. The pioneering measurements collected by Moore *et al.* [22] showed the increases of the surface NRCS as a function of wind speed and rainrate. However, they also showed that raindrop sizes as distinct from the bulk rainrate can have a definite influence on the NRCS in controlled circumstances. As an example of the intricate complexity of all these relationship, the results in their Fig. 1 show that for the case of a 13 mm/hr rainfall (with a smaller droplet size), the NRCS value for their corresponding "D" curve is higher than that for the 3 mm/hr rainfall (the "F" curve) only until the wind speeds grows to 6 m/s. Then, the NRCS for this "D" curve becomes less than that for the lower rainrate. In addition, at wind speeds above 9 m/s, the NRCS becomes smaller than the no-rain condition, similar to what we see in some data points in Figs. 11 and 12. The implication this comparison here is to suggest that a great deal is unknown about the possible consequences of combinations of raindrop size distributions, wind speed, and bulk rainrate. For example, the rain-induced roughness also strongly depends on the drop's terminal velocity and the kinetic energy it transfers to the sea surface. Moderate winds will have a definitive impact on this energy transfer and the surface geometric features. It is not clear if these matters could explain the confusing features in Figs. 11 and 12, but they call attention to phenomena that deserve additional inquiry.

The results described in the preceding sections are found to be in general agreement with measurements made at the same frequency by Contreras *et al.* [5]. There are inherent differences in the time and spatial averages between these two experiments, and in the incidence angles of the radars. However there are notable similarities. In Fig. 13 of their paper, for the V-pol data at 51° incidence angle, there is good agreement between their measured NRCS (-15 dB) at a wind speed of 5 m/s and rainrate of 10 mm/hr and the results presented here in Figs. 15 and 16. Both studies find that the rainrate dependence is stronger at lower wind speeds. Little azimuth angle dependence is detected at the higher rainrates (> 5 mm/hr), but both data sets are limited in the azimuth angle range of values.

The results in Figs. 13–16 are based on the lower wind conditions in Box #1. These provide new specific knowledge about the rainrate dependence, without attributes that are inconsistent with previous studies. It is anticipated that these results will be the initial phase of the expansion of our empirical and physical knowledge of this interesting remote-sensing problem. Since scatterometers are widely believed to respond to stress rather than wind, it would be very interesting to examine the impact of rain as a function of surface turbulent stress rather than wind. Such a contribution would be useful for ocean modeling related to climate as well as ocean and atmospheric studies of severe weather. In order to develop useful models for satellite applications this program will continue to study rain-induced modifications as a function of wind speed, rainrate (drop

size distribution), and azimuth angle. With this information, it should be possible to improve estimates of scatterometer-derived wind speed and related air-sea interactions.

APPENDIX
ELECTROMAGNETIC MODEL OF THE NRCS (σ_{ax}) MEASURED BY THE SWS AND RAIN IMPACT NRCS, σ_{rn0}

Use of "x" subscript below will represent either "h" or "v" polarization.

σ_{ax} total measured NRCS at receiver; sum of contributions from sea surface and rain volume;

σ_{wdx} sea surface radar cross section due to wind driven roughness alone (wind-NRCS);

σ_{rnx} sea surface radar cross section due to rain impact roughness alone (rain-NRCS);

$\alpha_{\mathrm{x}}(\mathrm{r})$ attenuation, in nepers/meter for each polarization, function of local volume rainrate or precipitation water content;

$\sigma_{\mathrm{ox}}(\mathrm{r})$ surface equivalent of volumetric rain RCS, $=$ constant $*\ \mathrm{Z_x}$ (the radar reflectivity factor for $\mathrm{K_u}$-band, $\mathrm{Z_x}$, varies with position, "r");

lenx path length of radar beam for each polarization $=$ $\mathrm{len}/\mathrm{Cos}(\theta_{\mathrm{x}})$ (rain column height, over scatterometer footprint $=$ len, $\theta_{\mathrm{h}} = 46^\circ$ and $\theta_{\mathrm{v}} = 54^\circ$);

$$\sigma_{\mathrm{ax}} = \int_0^{\mathrm{lenx}} \sigma_{\mathrm{ox}} e^{-4\int_r^{\mathrm{lenx}} \alpha_{\mathrm{x}}(s)ds}\, dr + (\sigma_{\mathrm{wdx}} + \sigma_{\mathrm{rnx}}) * e^{-4\int_0^{\mathrm{lenx}} \alpha_{\mathrm{x}}(s)ds} \quad (1)$$

σ_{rn0} model function for the NRCS due to rain impact; depends on wind magnitude and rainrate.

After solving for the total surface NRCS $= (\sigma_{\mathrm{wdx}} + \sigma_{\mathrm{rnx}})$ from a rain affected area, the wind-driven term alone is estimated from a nearby rain-free area: σ_{wdx}. Then, their ratio σ_{rn0} is computed, producing

$$\sigma_{\mathrm{rn0}} = \left(\frac{\sigma_{\mathrm{wdx}} + \sigma_{\mathrm{rnx}}}{\sigma_{\mathrm{wdx}}}\right). \quad (2)$$

ACKNOWLEDGMENT

The authors would like to thank several colleagues for their significant contributions and advice during the conduct of these investigations. Dr. S. Durden (Jet Propulsion Laboratory) contributed calculations of raindrop radar cross sections at both polarizations for $\mathrm{K_u}$-band. Dr. D. Long (Brigham Young University) contributed algorithms that calculated the beam shape and illumination of the QuikSCAT antennas. J. Tongue and M. Istok (NWS) provided the software and related resources essential to accessing the NEXRAD Level-II data. G. Apgar (Hofstra University) developed the algorithms converting the NEXRAD data into 3-D Cartesian reflectivity. Dr. S. Hristova-Veleva (Jet Propulsion Laboratory) provided valuable insights for the calculations of volume reflectivity and beam attenuation. The QuikSCAT Level 2A data was provided by the NASA Jet Propulsion Laboratory PO.DAAC.

REFERENCES

[1] D. Atlas and C. Ulbrich, "Drop size spectra and integral remote sensing parameters in the transition from convective to stratiform rain," *Geophys. Res. Lett.*, vol. 33, no. 16, L16 803, Aug. 2006. DOI:10.1029/2006GL026824.

[2] L. F. Bliven and J. P. Giovanangeli, "An experimental study of microwave scattering from rain- and wind-roughened seas," *Int. J. Remote Sens.*, vol. 14, no. 5, pp. 855–869, Mar. 1993.

[3] N. Braun and M. Gade, "Multi-frequency scatterometer measurements on water surfaces agitated by artificial and natural rain," *Int. J. Remote Sens.*, vol. 27, no. 1/2, pp. 27–39, Jan. 2006.

[4] D. B. Chelton, M. G. Schlax, M. H. Freilich, and R. F. Milliff, "Satellite measurements reveal persistent small-scale features in ocean winds," *Science*, vol. 303, no. 5660, pp. 978–983, Jan. 15, 2004.

[5] R. F. Contreras, W. J. Plant, W. C. Keller, K. Hayes, and J. Nystuen, "Effects of rain on Ku-band backscatter from the ocean," *J. Geophys. Res.*, vol. 108, no. C5, pp. 34-1–34-13, May 2003.

[6] R. F. Contreras and W. J. Plant, "Surface effect of rain on microwave backscatter from the ocean: Measurements and modeling," *J. Geophys. Res.*, vol. 111, no. C8, C08 019, Aug. 2006. DOI:10.1029/2005JC003356.

[7] C. Craeye, "Radar signature of the sea surface perturbed by rain," Ph.D. dissertation, Univ. Catholique Louvain, Lab. Telecommun. Teledetection, Louvain-la-Neuve, Belgium, 1998.

[8] T. D. Crum and R. L. Alberty, "The WSR-88D and the WSR-88D operational support facility," *Bull. Amer. Meteorol. Soc.*, vol. 74, no. 9, pp. 1669–1687, Sep. 1993.

[9] R. J. Doviak and D. S. Zrnic, *Doppler Radar and Weather Observations*, 2nd ed. San Diego, CA: Academic, 1993.

[10] D. W. Draper and D. G. Long, "Evaluating the effect of rain on SeaWinds scatterometer measurements," *J. Geophys. Res.*, vol. 109, no. C2, C02 005, Feb. 15, 2004.

[11] D. W. Draper and D. G. Long, "Simultaneous wind and rain retrieval using SeaWinds data," *IEEE Trans. Geosci. Remote Sens.*, vol. 42, no. 7, pp. 1411–1423, Jul. 2004.

[12] S. L. Durden, Z. Haddad, A. Kitiyakara, and F. K. Li, "Effects of nonuniform beam filling on rainfall retrieval for the TRMM precipitation radar," *J. Atmos. Ocean. Technol.*, vol. 15, no. 3, pp. 635–646, Jun. 1998.

[13] S. L. Durden, private communication, 2003.

[14] M. Freilich, "SeaWinds Ku-band scatterometer measurements: Characteristics and challenges," in *Proc. NOAA/NASA Workshop Satellite Meas. Ocean Vector Winds*, Miami, FL, Feb. 8–10, 2005.

[15] J. Goldhirsh and B. Musiani, "Rain cell size statistics derived from radar observations at Wallops Island, Virginia," *IEEE Trans. Geosci. Remote Sens.*, vol. GRS-24, no. 6, pp. 947–954, Nov. 1986.

[16] Z. S. Haddad, D. A. Short, S. L. Durden, E. Im, S. Hensley, M. Grable, and R. A. Black, "A new parametrization of the rain drop size distribution," *IEEE Trans. Geosci. Remote Sens.*, vol. 35, no. 3, pp. 532–539, May 1997.

[17] JPL, *QuikSCAT Science Data Product User's Manual*, Sep. 2006, JPL/California Inst. Technol./NASA, Version 3.0, D-18053-Rev A.

[18] G. E. Klazura and D. A. Imy, "A description of the initial set of analysis products available from the NEXRAD WSR-88D system," *Bull. Amer. Meteorol. Soc.*, vol. 74, no. 7, pp. 1293–1311, Jul. 1993.

[19] D. G. Long, private communication, 2005.

[20] R. Meneghini and T. Kozu, *Spaceborne Weather Radar*. Boston, MA: Artech House, 1990, 199 pp.

[21] R. F. Milliff, J. Morzel, D. B. Chelton, and M. H. Freilich, "Wind stress curl and wind stress divergence biases from rain effects on QSCAT surface wind retrievals," *J. Atmos. Ocean. Technol.*, vol. 21, no. 8, pp. 1216–1231, Aug. 2004.

[22] R. K. Moore, Y. S. Yu, A. K. Fung, D. Kaneko, G. J. Dome, and R. E. Werp, "Preliminary study of rain effects on radar scattering from water surfaces," *IEEE J. Ocean. Eng.*, vol. OE-4, no. 1, pp. 31–32, Jan. 1979.

[23] C. Schumacher and R. A. Houze, "Stratiform rain in the tropics as seen by the TRMM precipitation radar," *J. Climate*, vol. 16, no. 11, pp. 1739–1756, Jun. 2003.

[24] B. W. Stiles, private communication, 2007.

[25] D. E. Weissman, M. A. Bourassa, and J. Tongue, "Effects of rain rate and wind magnitude on SeaWinds scatterometer wind speed errors," *J. Atmos. Ocean. Technol.*, vol. 19, no. 5, pp. 738–746, May 2002.

[26] D. E. Weissman, M. A. Bourassa, J. J. O'Brien, and J. Tongue, "Calibrating the QuikSCAT/SeaWinds radar for measuring rainrate over the oceans," *IEEE Trans. Geosci. Remote Sens.*, vol. 41, no. 12, pp. 2814–2820, Dec. 2003.

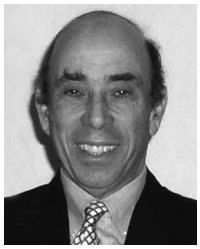

David E. Weissman (S'60–M'61–SM'76–F'91–LF'03) received the B.A. and B.E.E. degrees and the M.E.E. degree from New York University, New York, in 1960 and 1961, respectively, and the Ph.D. degree in electrical engineering from Stanford University, Stanford, CA, in 1968.

From 1963 to 1968, he was a Research Engineer with the Stanford Research Institute, Menlo Park, CA. Since 1968, he has been an Electrical Engineering faculty member with Hofstra University, Hempstead, NY. His research, for over 40 years, has been involved in the development of microwave radar and radiometric remote-sensing techniques that can estimate ocean surface wind stress and the effect and amelioration of precipitation interference. These results, broadly published in the engineering and scientific literature, enable applications for satellite-based radars (SeaWinds on QuikSCAT and Advanced Earth Observing Satellite-2). These efforts, supported by the NASA Physical Oceanography Program, are part of the Ocean Vector Winds Science Team, with collaborations from Florida State University, Tallahassee, and the New York City office of National Weather Service. His service to the IEEE spans over 35 years.

Dr. Weissman received the National Research Council Senior Postdoctoral Associateship in 1974 to 1975 at the NASA Jet Propulsion Laboratory. He was elected IEEE Fellow, in December 1990. He received the IEEE Centennial Medal in 1984 (nominated by the Oceanic Engineering Society). He received the Best Applications Paper Award in 1977 for a paper coauthored with James W. Johnson published in the IEEE TRANSACTIONS ON ANTENNAS AND PROPAGATION. He was honored with the Oceanic Engineering Society Distinguished Service Award in 1995. He received the NASA HQ Citation for Contributions to the NSCAT Scatterometer Project in 1998. He was Editor-in-Chief of the IEEE JOURNAL OF OCEANIC ENGINEERING from 1979 to 1982 and has been a member of the Administrative Committee (ADCOM) of the Oceanic Engineering Society since 1976. He has been Chairman of the Technical Committee on Remote Sensing, Oceanic Engineering Society (OES) since 1985 and is currently Chairman of the OES Fellow Evaluation Committee. Since his election to the Geoscience and Remote Sensing ADCOM in 1999, he has been serving as Education Committee Chair and is currently the Publicity and Public Relations Coordinator. In December 2006, he received a Grant from the IEEE Foundation to initiate a new type of collaboration: one between experts within IEEE technical societies [specifically Geoscience and Remote Sensing Society (GRSS)] and museums, with the purpose of creating new types of museum exhibits that can better display activities that engineers engage in, to students and the general public. This resulted in a Weather Radar Exhibit which is now on display at the Cradle of Aviation Museum, Garden City, NY.

Mark A. Bourassa received the B.Sc. degree in physics and the M.Sc. degree in meteorology from the University of Alberta, Edmonton, AB, Canada, in 1985 and 1989, respectively, and the Ph.D. degree in atmospheric sciences from Purdue University, West Lafayette, IN, in 1993.

From 1994 to 1995, he was an Office of Naval Research Postdoctoral Fellow with the Air–Sea Interaction Laboratory, University of Delaware, Newark. He is currently an Associate Professor with the Department of Meteorology, Florida State University, Tallahassee, and is a member of the Center for Ocean–Atmospheric Prediction Studies and the Geophysical Fluid Dynamics Institute. His main research interests are air–sea interaction, remote sensing related to air–sea interaction and precipitation, and data fusion. His interests in air–sea interaction and remote sensing have been combined in studies of scatterometry since 1996, when he began to work with data from the NASA scatterometer (NSCAT). He now uses *in situ* and remotely sensed observations, combined with models of the atmospheric boundary layer, to better understand air–sea interaction and the surface characteristics to which a scatterometer responds.

Dr. Bourassa is a member of the IEEE Geoscience and Remote Sensing Society, the American Geophysical Union, and the American Meteorological Society.